Materials Today Chemistry 34 (2023) 101789

Contents lists available at ScienceDirect

Materials Today Chemistry

journal homepage: www.journals.elsevier.com/materials-today-chemistry/

Reaching a near zero radiative heat transfer by the inclusion of modified multiwalled-carbon nanotubes (MWCNTs) in polyurethane-polyisocyanurate aerogels

Beatriz Merillas [a,*], Tomás Enrique Gómez Álvarez-Arenas [b], Fernando Villafañe [c], Miguel Ángel Rodríguez-Pérez [a,d]

[a] Cellular Materials Laboratory (CellMat), Condensed Matter Physics Department, Faculty of Science, University of Valladolid, Campus Miguel Delibes, Paseo de Belén 7, 47011, Valladolid, Spain
[b] Instituto de Tecnologías Físicas y de la Información, CSIC, C/Serrano 144, 28006, Madrid, Spain
[c] GIR MIOMeT-IU Cinquima-Química Inorgánica. Faculty of Science, University of Valladolid, Campus Miguel Delibes, Paseo de Belén 7, 47011, Valladolid, Spain
[d] BioEcoUVA Research Institute on Bioeconomy, University of Valladolid, Spain

ARTICLE INFO

Keywords:
Carbon nanotubes
Polyurethane aerogels
Thermal insulation
Radiative contribution
Mechanical properties

ABSTRACT

This article studies the effect of adding different contents of surface-modified multiwalled carbon nanotubes (CNTs) on the structure and final properties of polyisocyanurate-polyurethane aerogels. The produced samples were characterized in terms of density, porosity, shrinkage, textural properties, mechanical behavior, ultrasonic behavior, and thermal conductivity. Low-weight aerogels were obtained with densities between 89 and 95 kg/m^3. The inclusion of homogeneously dispersed carbon nanotubes protected the aerogel structure during supercritical drying decreasing the final shrinkage of these samples and, therefore, increasing their porosity. The porous structure of the aerogels containing CNTs was modified, and slightly larger pores were formed. The structural modifications contribute to decrease the stiffness of the samples while improving their resilience and elasticity. Finally, a significant enhancement on the insulating performance of the aerogels has been found when CNTs were added reaching values as low as 12 mW/mK. These fillers were proved to act as infrared opacifiers by absorbing and scattering the infrared radiation, a relevant contribution in these lightweight materials. In fact, the radiation contribution was strongly reduced when the content of CNTs reached 3 wt%, being this contribution near zero. Thus, this content was considered as the optimum for the final properties-balance in these aerogels.

1. Introduction

In the recent years, the promising properties that aerogels provide have placed them at the top of the search for novel materials. Their low density, high porosity (80–99.8 %) and surface areas (500–1200 m^2/g) [1], in combination with other properties such as a low refraction index (~1.05) and heat and sound insulating capacity, make them suitable candidates for a wide range of applications. The inclusion of different fillers to enhance specific properties is an interesting strategy that has been used in aerogels. Among the different fillers used for aerogels, sepiolite fibers [2,3], nanoclays [4], different fibers (natural, man-made, organic, inorganic and nanofibres) [5,6], and carbon-based fillers are commonly used.

Focusing on the last fillers (carbon-based fillers), there are several outstanding publications that are worthy to be mentioned. Loche et al. [7] incorporated graphene to silica aerogels aiming to increase the hydrophobicity of these materials. A significant enhancement was found, and in fact, graphene/silica aerogels were able to selectively uptake oil from oil-water mixtures. Dervin et al. [8] included graphene oxide in ambient pressure dried, hydrophobic silica aerogels. The authors obtained a significant increase in the surface area (from 390 to 700 m^2/g) and pore volume (from 0.59 to 0.99 cm^3 for samples of the same volume), while decreasing the aerogel density in the case of 0.5 wt% of GO. It was observed that the intercalation of GO within the silica matrix contributed to reduce the volume shrinkage during the drying step, allowing to enhance the physical properties of the final aerogels. Lamy-Mendes et al. [9,10] added carbon nanotubes (CNTs) and graphene oxide (GO) in different silica aerogel formulations based on

* Corresponding author.
E-mail addresses: b.merillas@fmc.uva.es, beatriz.merillas@uva.es (B. Merillas).

https://doi.org/10.1016/j.mtchem.2023.101789
Received 12 August 2023; Received in revised form 20 October 2023; Accepted 21 October 2023
Available online 25 October 2023

methyltrimethoxysilane (MTMS) and 3-aminopropyltrimethoxysilane (APTMS) and studied their effect on the microstructure and physical properties. They found a clear effect on the silica growth, leading to changes in the aerogel's microstructure. In addition, their elastic modulus was significantly increased as well as the thermal insulation. Piñero et al. [11] used carbon nanotubes as reinforcement of silica aerogels reaching an improvement of their compressive strength by 50 %. Teymouri et al. [12] produced polyurethane nanocomposite aerogels with multiwalled carbon nanotubes obtaining a significant increase in the storage modulus and recovery ratio (180 % and 42 %, respectively) with respect to the pure aerogel. This improvement was reached for a nanoparticle amount beyond the percolation threshold, which was 2.75 wt% for that system.

Carbon nanotubes (CNTs) are cylinder-shaped allotropic forms of carbon that are well-known to block the infrared radiation [13,14]. Taking into account that radiative heat transfer is a contribution to the total thermal conductivity in porous materials [15], by setting several infrared absorption nuclei in a porous structure, the insulating performance could be enhanced. For instance, Santiago et al. [16] added different contents of carbon nanofibers in water-blown rigid polyurethane foam formulations reporting that they promote a clear reduction in the radiative contribution by increasing the extinction coefficient and, therefore, thermal conductivity was reduced by a 2.2 %.

Therefore, herein, the inclusion of multi-walled carbon nanotubes is the selected method to improve the thermal insulating performance of polyurethane-polyisocyanurate aerogels that already presented very low values of the thermal conductivity of 15 mW/mK. The choice of polyurethane aerogels is based on their improved mechanical strength in comparison with other inorganic aerogels [17], as well as the wide possibilities for chemical modifications. As far as the authors know, there are no previous publications dealing with the effect of adding carbon nanotubes on organic super-insulating aerogels based on polyurethane-polyisocyanurate, constituting thus an innovative strategy for these materials. The possible influence of these fillers in the aerogel structure has been evaluated by different techniques. Moreover, a detailed study of the effect of these fillers in the different contributions to the total thermal conductivity was performed, reaching clear conclusions about the mechanisms in which CNTs are involved.

For it, the propagation of sound through the aerogel was measured, allowing to obtain more precise data of the conduction through the solid phase contribution. As a result of this research, polyurethane-based aerogels with reduced thermal conductivities and higher elasticity have been produced.

2. Experimental section

2.1. Materials

Isocyanate IsoPMDI 92140 (p-MDI) ($\rho = 1.23$ g/cm^3), was obtained from BASF Polyurethane. Pentaerythritol ($\rho = 1.396$ g/cm^3) was provided by Alfa Aesar. KOSMOS 75 MEG was employed as catalyst and was supplied by Evonik. Commercial multi-walled carbon nanotubes (CNTs, purity 90 %) were provided by Nanocyl. Tetramethylorthosilicate (TMOS, $Si(OCH_3)_4$) (purity ≥99 %) was obtained from Sigma Aldrich.

Scharlab, S. L. supplied the following solvents: acetone (purity >99.5 %), acetonitrile (purity >99.9 %), DMSO (purity >99.5 %) and tetrahydrofurane (purity >99.5 %) stabilized with 250 ppm BHT. Nitric acid (purity 70 %) was obtained from Sigma Aldrich.

2.2. CNTs surface modification

Following the procedure described by Kim et al. [18], carbon nanotubes were modified by refluxing with concentrated nitric acid for 20 h at 50 °C. Then, CNTs were filtered and washed with water several times until collecting a neutral pH solution. After washing, the fillers were dried at 60 °C overnight. Finally, a silane treatment was performed by refluxing for 4 h at 70 °C with a silane solution (10 % TMOS in 70 % ethanol/30 % water) and drying at 60 °C overnight.

2.3. Synthesis of aerogels with CNTs as fillers

Polyurethane-polyisocyanurate aerogels are synthesized by polymerization between isocyanate and polyol [19]. First, the corresponding amount of CNTs (0.5, 1.0 and 3.0 wt% over the total sum of polyol and isocyanate mass) is added to the isocyanate solution (44 g/L in CH_3CN 75 % vol./THF 35 % vol.) and the mixture is ultrasonicated for 30 min with an ultrasonic bath (Retsch GmbH, Germany). By mixing a solution of pentaerythritol (100 g/L in DMSO) with the isocyanate-carbon nanotubes solution in presence of a 4 wt% (weight over the total polyol and isocyanate mass) of catalyst a sol is formed. Once the catalyst is quickly added, this solution was continuously stirred at 300 rpm through magnetic stirring in the corresponding container until the gel formation. When the gel is almost formed, the magnetic stirrer was quickly removed from the container. Different containers were used for obtaining samples with different dimensions. Samples for thermal conductivity were produced in plastic containers, obtaining cylinders of ca. 40 mm diameter and 15 mm height. Samples for mechanical tests were produced in plastic syringes obtaining gels of ca. 17 mm diameter and 9 mm height.

During the gelation, viscosity progressively increases, and the solution color is notably changed until reaching the gelation point in which gel does not flow. Then, gels were aged for 24 h by covering them with pure acetonitrile, and then washed twice each 24 h with the same solvent. Finally, gels were dried by the supercritical drying method at 40 °C and 100 bar.

2.4. Characterization techniques

2.4.1. Gelation time

The time in which gelation has finished was taken as the time when the gel color changes to whitish and viscosity reaches the maximum, not being possible to flow by tilting the container.

2.4.2. Bulk density, relative density and porosity

Bulk density was obtained as the ratio between mass and geometrical volume as described in ASTM D1622/D1622M − 14 [20]. Relative density was calculated as follows:

$$\rho_r = \frac{\rho}{\rho_s} \tag{1}$$

Where ρ the geometric density and ρ_s the solid density, i.e. 1.17 g/cm^3 measured by helium pycnometry [19].

Porosity (Π) accounts for the gaseous fraction of the aerogels and was calculated by equation (2):

$$\Pi = (1 - \rho_r) * 100 \tag{2}$$

2.4.3. Shrinkage

The shrinkage that samples experimented during drying was measured both, lineally and volumetrically, by measuring the diameter and volume of the gels before and after drying:

$$S_l(\%) = \left(1 - \frac{d}{d_0}\right) \cdot 100 \tag{3}$$

$$S_v(\%) = \left(1 - \frac{V}{V_0}\right) \cdot 100 \tag{4}$$

where d_0 and V_0 are the diameter and volume, respectively, of gels before drying, and d and V are the diameter and volume of aerogels after drying.

2.4.4. Scanning electron microscopy and transmission electron microscopy

Aerogels nanostructure was observed by means of a scanning electron microscope (ESEM Scanning Electron Microscope QUANTA 200 FEG, Hillsboro, OR, USA). Prior to the visualization, samples were metallized with iridium to avoid modifications of the aerogel morphology [21]. Particle diameter was measured with the Image J/FIJI software [22], and the normalized standard deviation (with the average diameter) was calculated.

CNTs were observed by Transmission Electron Microscopy (TEM) with a JEOL JEM1011 microscope at the Instrumental Techniques Laboratory from the Scientific Park of the University of Valladolid by placing the nanotubes on a carbon tape. The nanotube diameter was measured with the Image J/FIJI software [22].

2.4.5. Infrared spectroscopy

Infrared spectra were collected using a Bruker Tensor 27 FTIR spectrometer. Infrared spectroscopy was employed to identify the characteristic functional groups of the carbon nanotubes. After deducing a background spectrum, spectra were obtained with 32 scans with a resolution of 2 cm^{-1} in a wavelength range from 400 to 4000 cm^{-1}.

2.4.6. Specific surface area (S_{BET})

Nitrogen sorption (Micromeritics ASAP 2020 instrument) measurements were performed in the University of Málaga (Spain). Aerogels were initially degassed under vacuum at 25 °C for 24 h and then experiments were carried out at – 196 °C in the range $P/P_0 = 0.05–0.30$. The specific surface area was obtained by the Brunauer-Emmett-Teller (BET) method [23].

2.4.7. Particle size, pore volume and pore size

Particle size ($\varphi_{particle}$) was measured from the SEM micrographs by drawing the particle contour with a software based on Image J/FIJI [22]. More than 50 particles were analyzed for obtaining an average value of the particles size.

Pore volume was calculated as the gaseous volume per unit of mass through equation (6):

$$V_p = \frac{1}{\rho} - \frac{1}{\rho_s} \tag{6}$$

Pore size was measured through the Barrett–Joyner–Halenda (BJH) method [23] and assuming cylindrical pores:

$$\Phi_{pore} = \frac{4V_p}{S_{BET}} \tag{7}$$

2.4.8. Optical transmittance measurements

Transmittance measurements were carried out by using a red laser (650 nm) obtained from Laserlince S.L. (Valladolid, Spain). Additionally, an integrating sphere with 12.5 mm window (PRW0505, Gigahertz-Optik) connected to a photometer (X94, Gigahertz-Optik, Türkenfeld, Germany) was used as detector. Transmittance was calculated as the ratio between the intensity reaching the detector through the aerogel sample (I) and raw intensity emitted by the laser. Samples were placed as close as possible to the integrating sphere. The transmittance measurements were normalized to a selected thickness of 2 mm (L) through the following equation:

$$T = T_O^{\frac{L}{L_0}} \tag{8}$$

Where T_0 corresponds to a reference transmittance value, L_0 is the real sample thickness, and L is the selected thickness to calculate the transmittance.

2.4.9. Thermal conductivity measurements

Thermal conductivity was obtained by the steady state method through a heat flow meter model FOX 314 (TA Instruments/LaserComp, Inc.), which measures according to ASTM C518 [24], and ISO 8301 [25]. The equipment has been adapted for measuring small samples by including an external heat flux sensor gSKIN® XM 27 9C (greenTEG AG) connected to a data logger gSKIN® DLOG-4219 (greenTEG AG) as described by Sanchez-Calderón et al. [26].

These measurements were performed at 10, 20, 30, and 40 °C, keeping a temperature gradient of 20 °C on each measurement.

2.4.10. Speed of sound measurements

The experimental set-up consists on a pair identical of non-focused air-coupled ultrasonic transducers (developed at ITEFI-CSIC), centre frequency 500 kHz, −20 dB relative bandwidth of 75 % and 20 mm aperture. Transducers are operated in through transmission mode, located in opposition at a distance of 70 mm. The aerogel sample is placed in between them at normal incidence. Transmitter transducer is driven by a Panametrics 5077 pulser-receiver (P/R) that generates a semicycle of square wave, amplitude – 200V, tuned at transducers center frequency, with pulse repetition frequency (PRF) set to 100 Hz. Received signal in the receiver transducers is amplified in the receiver stage of the 5077 (up to 40 dB) and is then transferred to a Tektronix 5054 digital oscilloscope where it is digitized, displayed, and stored (sampling frequency 10 MS/s, record length 10k), using an averaging of 126 waveforms to improve the signal to noise ratio. Oscilloscope trigger source signal is provided by the 5077 P/R synchronism output signal (TTL). Signals received in the received transducer with and without sample between the transducers were acquired. Ultrasound velocity in the sample (v) is then obtained from the velocity in the air (v_{air}), the sample thickness (d) and the difference of time of flight in both cases (Δt) as indicated in equation (9).

$$v = \frac{d}{\Delta t + d/v_{air}} \tag{9}$$

Where the difference in the time of flight can be calculated from the edge detection or the maximum in the cross-correlation between both signals or the phase difference. A photograph of the set-up and one example is shown in Fig. 1. The transmitted signal received with the aerogel sample between the transducers is delayed with respect to the signal received without sample because the ultrasound velocity in the aerogel is lower that then velocity in the air.

2.4.11. Mechanical tests

Compression tests were performed by an universal testing machine (Instron model 5500R6025) according to the standard ASTM D1621-00 [27] at room conditions (23 ± 2 °C and 50 ± 10 % of relative humidity as indicated by ISO 291:2005 [28]. All samples were conditioned for 24 h before evaluation. The displacement rate was [height/10] mm/min and a load cell of *ca.* 1 kN was used.

Five loading-unloading cycles at a strain up to 10 % were performed allowing to calculate the energy loss coefficient (ELC) from the hysteresis area [29]:

$$ELC\ (\%) = \frac{A_L - A_U}{A_L} \cdot 100 \tag{10}$$

Where A_L and A_U are the areas under the loading and unloading curve, respectively.

The elastic modulus (E) was calculated from the slope of the linear region of the compression curves.

After these cycles, an additional experiment until reaching a strain of ca. 80 % was performed.

3. Results and discussion

This section comprises the obtained results regarding the synthesis and characterization of the polyisocyanurate-polyurethane aerogels containing carbon nanotubes as fillers.

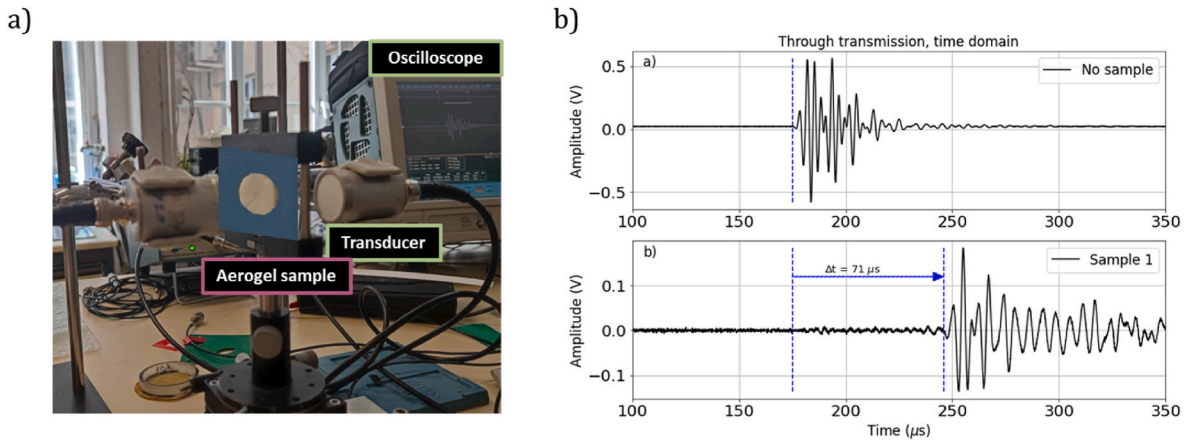

Fig. 1. a) Set-up for the sound measurements, b) Received signal in the receiver transducer: up) no sample between transducers, down) sample between transducers at normal incidence.

3.1. Carbon nanotubes

After the modification of the carbon nanotubes, these fillers were characterized by FT-IR and TEM. Fig. 2 a represents the infrared spectrum where the chemical bonds promoted during the silane treatment can be identified. The Si–O stretching vibration can be found at 515 and 900 cm^{-1} [30], a peak corresponding to the Si–O–Si bending at 1020 cm^{-1}, and the O–H stretching (Si–O–H) at 3800 cm^{-1} [31]. Therefore, the silane treatment was successful.

Fig. 2 b gathers two transmission electron micrographs of the carbon nanotubes dispersed along the carbon tape. The average diameter was measured after the silane modification obtaining a value of ca. 14.31 ± 1.25 nm, larger than the average diameter of the commercial carbon nanotubes [10] (9.5 nm) because of the incorporation of the silane compound on the surface. The average length of the studies nanotubes was 1.5 ± 0.2 μm.

3.2. Aerogel characterization

Some photographs of the sol-gel process can be found in Fig. 3 a, showing the color change in the appearance of the initial sol when gelation takes place. Starting from a yellowish solution, whitish color progressively appears with time until reaching an opaque color and a gel consistence characterized by a higher viscosity. The obtained gels (Fig. 3 b) containing carbon nanotubes showed a bluish color that the pure reference does not show. The reason behind could be changes in the nanostructure of these materials combined with the black color of the fillers. The gelation time was reduced by the addition of CNTs, decreasing from 5.50 min to 2.42 and 2.43 for the amounts of 0.5 and 1.0 wt%, respectively. The highest amount of 3.0 wt% showed a gelation time of 5.42 min, very similar to the value of the reference aerogel.

Once gels were dried, the obtained aerogels showed to be significantly homogeneous with few CNTs aggregates (Fig. 3 c).

Table 1 gathers the bulk density of the produced samples. The obtained values comprised between 89 and 95 kg/m^3. There does not exist an increasing effect of the carbon nanotube fillers on the final density due to the small amount included in each formulation. On the contrary, density is slightly reduced when CNTs are added because of the smaller shrinkage of the materials containing CNTs. Thus, relative densities of the aerogels with CNTs also decrease from 0.081 to 0.076, leading to higher porosities from 91.88 % for the reference to 92.36 % for the aerogel with the highest amount of CNT. This influence of carbon nanotubes can be observed in the linear and volumetric shrinkages that strongly decrease when carbon nanotubes are incorporated. For the linear shrinkage, the initial value of 11.82 % is reduced until 8.94 % and, in the case of the volumetric shrinkage, it drops from 52.71 % to 44.57 %, explaining the density reduction. Therefore, these fillers protect the aerogel structure during drying acting as rigid reinforcing points.

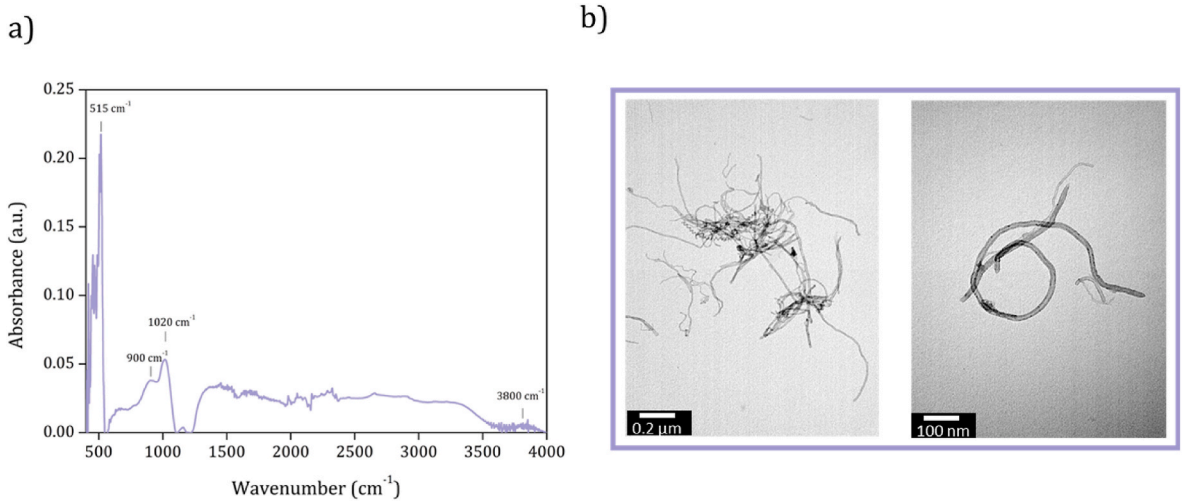

Fig. 2. a) Infrared spectrum and b) Scanning electron micrographs of the modified carbon nanotubes.

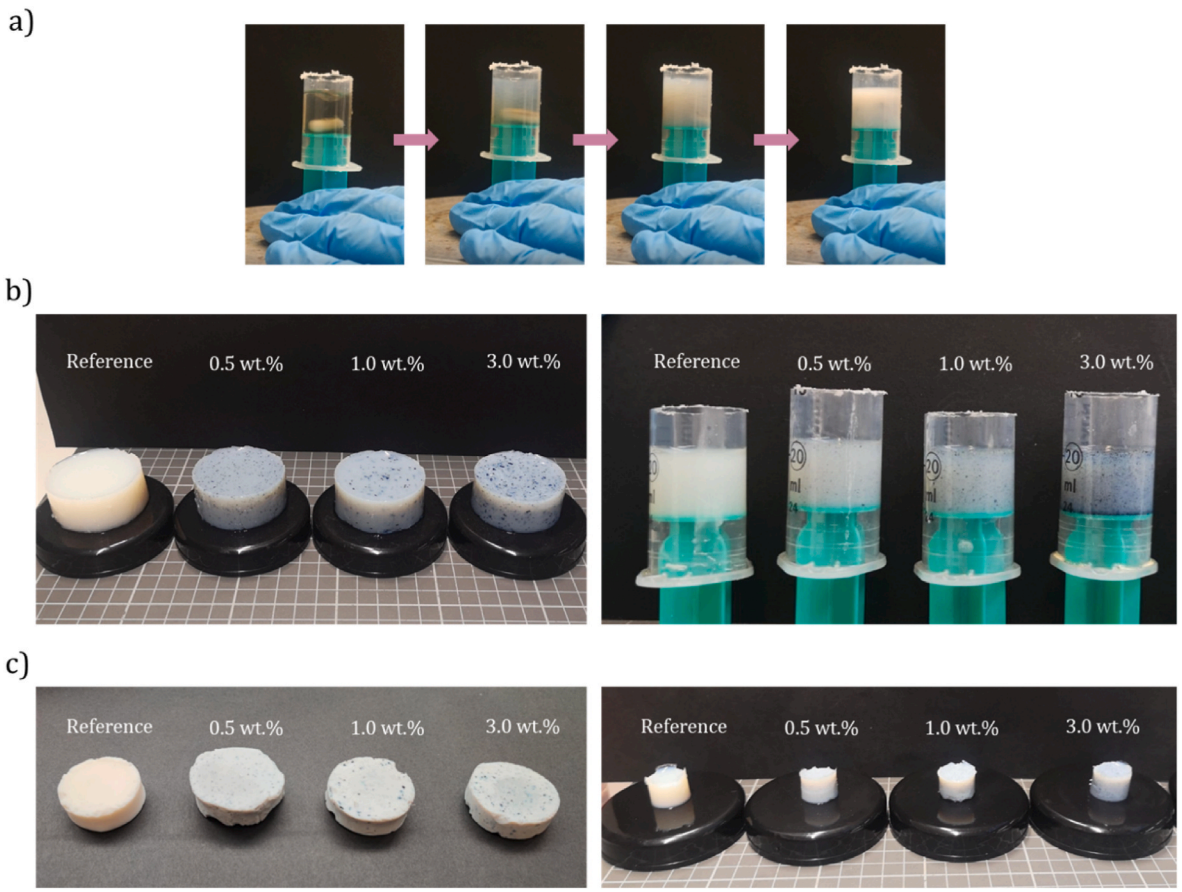

Fig. 3. a) photographs following the sol-gel process of one sample containing 0.5 wt% of CNTs, b) examples of gel samples for the thermal conductivity (left) and mechanical (right) measurements, c) examples of aerogel samples for the thermal conductivity (left) and mechanical (right) measurements.

Table 1
Main properties of the produced aerogels.

Sample	ρ_B (kg/m^3)	ρ_R	S_l (%)	S_v (%)	Π (%)	S_{BET} (m^2/g)	V_p (cm^3/g)	Mean pore size (nm)	$\varphi_{particle}$ (nm)	SD/$\varphi_{particle}$
Reference	95.05	0.081	11.82	52.71	91.88	255.02	9.67	151.61	49.05	0.190
0.5 wt% CNT	89.76	0.077	10.86	43.63	92.33	256.95	10.29	160.13	39.52	0.149
1.0 wt% CNT	91.28	0.078	12.17	49.66	92.20	237.16	10.10	170.36	42.62	0.147
3.0 wt% CNT	89.40	0.076	8.94	44.57	92.36	208.07	10.33	198.61	43.81	0.142

3.3. Porous structures

The porous structure of the produced aerogels has been studied by nitrogen sorption and scanning electron microscopy. The former provides information about the specific surface area, having notably high values of 255 m^2/g for the pure aerogel and 256, 237 and 208 m^2/g for the CNTs amounts of 0.5, 1.0 and 3.0 wt%, respectively. Taking into account this parameter and the pore volume per unit mass obtained from equation (6), the mean pore size was calculated. A clear trend is observed when adding CNTs as fillers: the higher the CNTs amount, the higher the pore size of the aerogels. This factor is correlated to the shrinkage that, as previously indicated, decreased for the samples containing CNTs. However, the increase in the pore size is mainly due to the decrease in the specific surface area of the aerogels when including the fillers. It can be explained by a different distribution of particles along the samples containing CNTs (probably along the carbon structures) leading to a different structural topology and, therefore, larger pores.

The scanning electron micrographs are included in Fig. 4. All of them showed a solid 3D network of nanometric particles forming interconnected strings. Carbon nanotubes could not be visualized by this technique and aggregates were not found along the examined samples, confirming the effective dispersion of the fillers.

The diameter of the particles forming the aerogel skeleton has been measured by drawing them with a specific software obtaining the values gathered in Table 1. These values are comprised between 49 and 39 nm, so all values are in the same range, but there exists a slight tendency to a reduction of the size of the particles forming the structure when carbon nanotubes are added. Additionally, the normalized standard deviation is also reduced by the CNTs incorporation accounting for a more homogeneous structure.

3.4. Transmittance measurements

Owing to the small features (particles and pores) forming the structure of these aerogels, and since the reference aerogel showed a significant transparency to visible light as described in our previous work [32], transmittance measurements have been carried out by using a red laser (650 nm) as light source and samples of 2 mm in thickness. The initial transmittance value for the reference was 42.1 % that was sharply reduced by the addition of carbon nanotubes to 15.5 % for 0.5 wt% CNTs, 14.8 % for 1.0 wt% CNTs, and 12.4 % for 3.0 wt% CNTs. This significant reduction was expected, and it is mainly due to the carbon

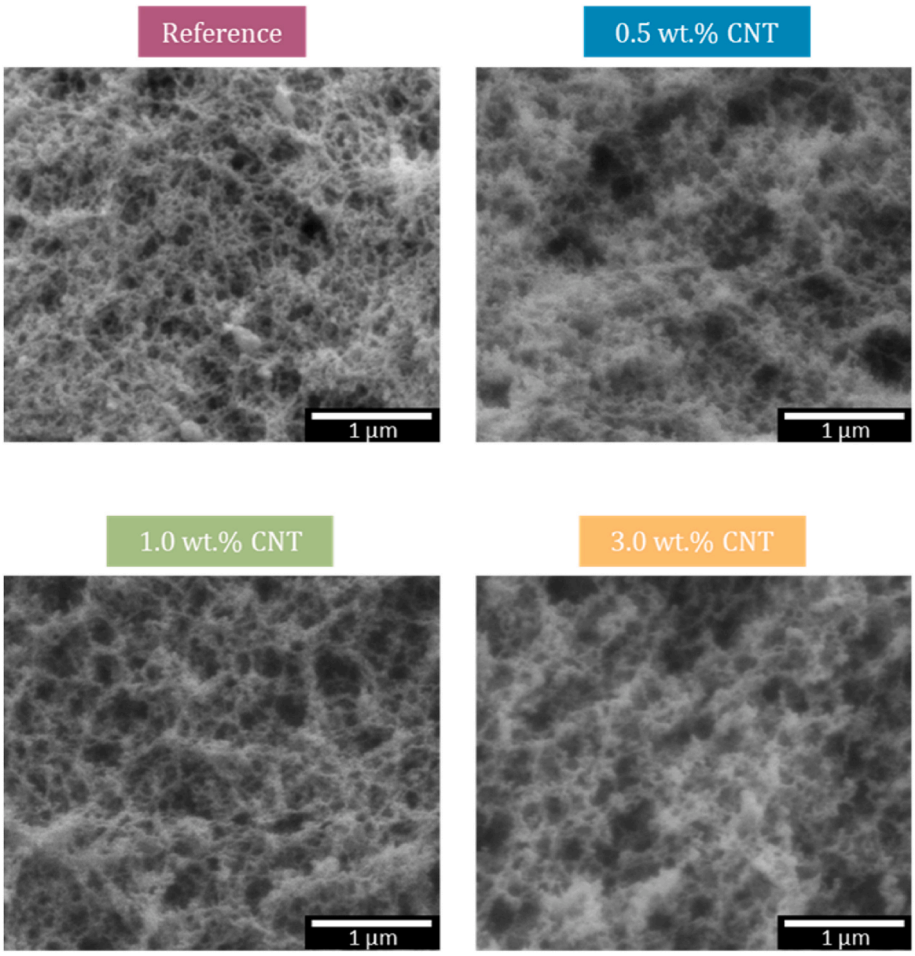

Fig. 4. Scanning electron micrographs of the aerogel samples.

nanotubes distributed along the nanoporous structure of the samples that act as absorption and scattering centers at visible wavelengths.

3.5. Mechanical properties

Different uniaxial compression tests were performed in order to evaluate the elasticity and stiffness of the produced aerogels. Five loading-unloading cycles until a strain of 10 % were carried out (Fig. 5) and the elastic modulus for each compression cycle was calculated (raw values at Supporting Information Table S1). Fig. 6 a shows that the elastic modulus of the reference aerogel is significantly higher than for the samples containing carbon nanotubes, reaching a value of 0.63 MPa. When carbon nanotubes are added, the elastic modulus is reduced to 0.30, 0.22 and 0.46 MPa. Since this reduction cannot be explained in terms of density, it could be due to a reduction in the size and strength of the interconnections between particles that may have a different structural distribution when CNTs are included, combined with the larger pores that are present in these samples. When larger voids are present, the aerogel particle-strings can be rearranged leading to a lower stiffness under an external force [33,34]. It is observed than the aerogel with the highest CNTs amount (3.0 wt%) experiments a slight increase in the elastic modulus in comparison with the aerogels containing a small amount of CNT. This behavior might be caused by the effect of the fillers that increase the stiffness of the polymer matrix. The obtained elastic moduli for the rest of cycles are similar to that of the first loading-unloading cycle, confirming that the produced aerogels can be loaded and unloaded several times without deteriorating its structure.

The hysteresis areas of the previous graphs (Fig. 5) have been measured accounting for the dissipated energy during the compression-decompression experiments. The calculated values are included in Table 2. The hysteresis area of the reference aerogel is higher for all the cycles meaning that a higher amount of energy is dissipated during the experiment and, therefore, this aerogel is less elastic. The aerogels containing 0.5 and 1.0 wt% of CNTs, as can be visually observed in Fig. 5, reached lower areas giving rise to more elastic aerogels. This characteristic could be related to the increased pore size of these samples that allow the solid skeleton to accommodate along these voids. Sample 3.0 wt% of CNTs shows a similar hysteresis area than the reference aerogel since, although pores reached the maximum size, the higher amount of carbon nanotubes is affecting the rigidity of the aerogel, as seen before with the elastic moduli (Fig. 6 a).

The aerogels under study were subjected to an experiment until higher deformations. The results are summarized in Fig. 6 b. Any sample was broken when high stress, more than 12 MPa, were applied. So, the aerogels show a tough behavior, completely different to the typical brittle behavior of inorganic aerogels.

The stresses applied at several levels of strain are analyzed in Fig. 7 (raw values can be found in Table S2). The initial stress for reaching a strain of 10 % was of 0.06 MPa for the reference aerogel. This value goes down until ca. 0.04 MPa for the samples with CNTs contents of 0.5 and 1.0 wt%. The sample with the highest CNTs content slightly increases this value to 0.05 MPa, therefore, not reaching the stiffness of the reference aerogel. At higher strains of 25, 50 and 75 % the same trend is observed: samples with low amounts of fillers (0.5 and 1.0 wt%.) present lower values of stress than the reference, whereas the aerogel with the highest content reaches similar values to the pure one.

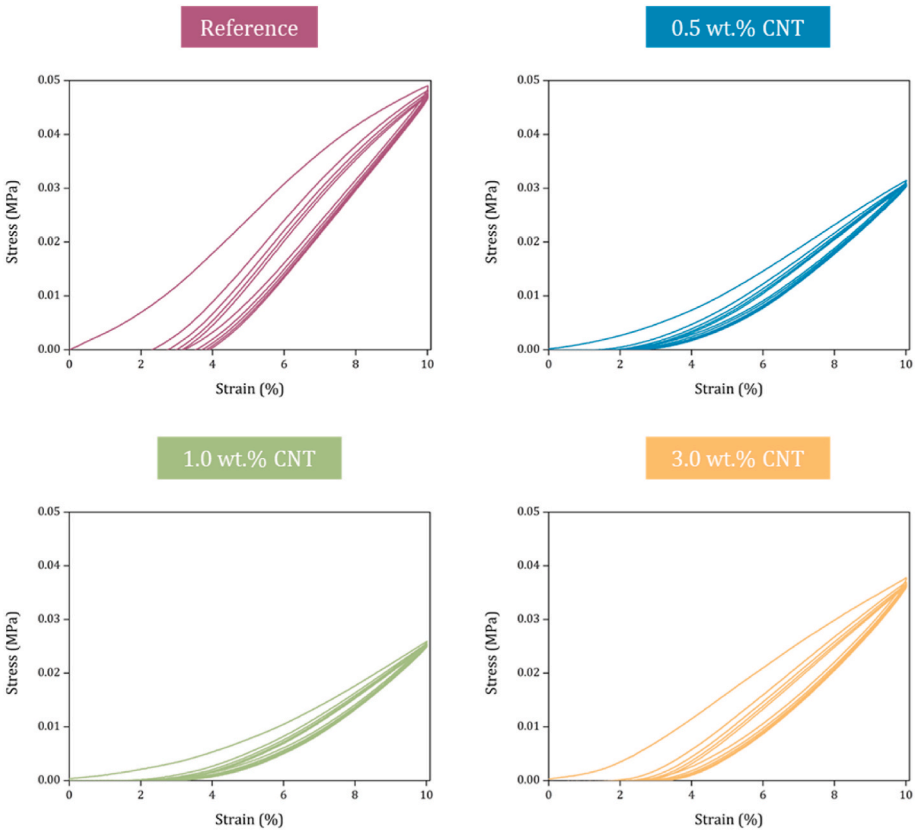

Fig. 5. Stress-strain plots for the loading-unloading cycles at a strain of 10 %.

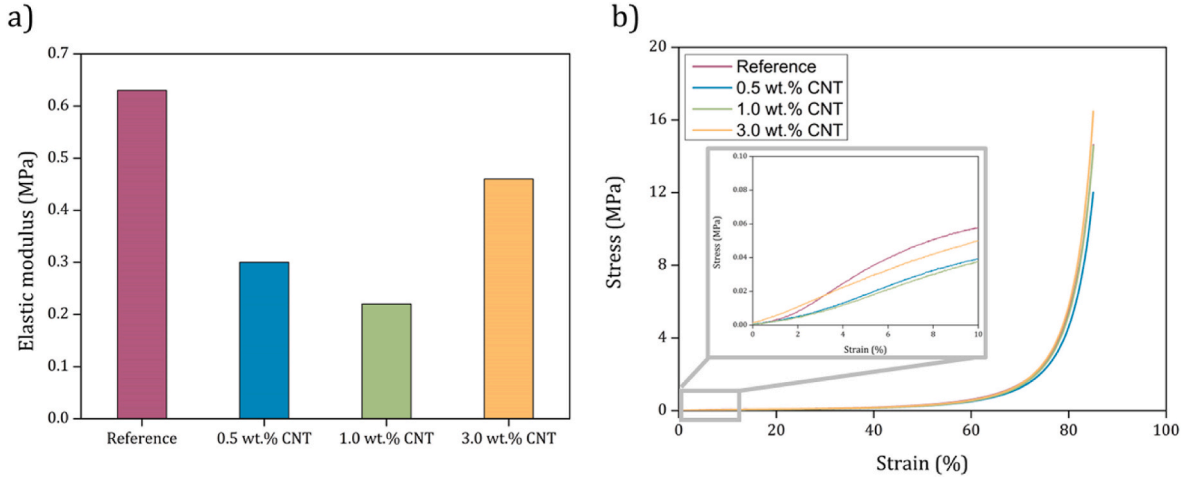

Fig. 6. a) Elastic moduli for the aerogels under study (first compression-decompression cycle), b) stress-strain curves for all the samples.

Table 2
Energy loss coefficient for all the compression-decompression cycles at a strain of 10 %.

Sample	ECL 1 (%)	ECL 2 (%)	ECL 3 (%)	ECL 4 (%)	ELC 5 (%)
Reference	39.71	25.24	22.82	21.67	19.84
0.5 wt% CNT	28.22	18.45	16.40	15.78	15.13
1.0 wt% CNT	30.26	18.35	16.72	15.76	14.96
3.0 wt% CNT	38.05	25.18	22.46	20.98	20.06

3.6. Speed of sound

The obtained signals in the ultrasound measurements (Fig. 8 a) clearly show that the inclusion of carbon nanotubes in the polyurethane aerogel causes a larger signal distortion while increasing the speed of sound (shorter time of flight). Therefore, their transmission coefficients were calculated (displayed in Fig. 8 b) indicating that, as expected, the increasing addition of these carbon fillers contributes to a larger sound transmission loss (STL) throughout the frequency range. In addition, the similar trend observed in all four cases suggests that the attenuation mechanism is similar in all cases.

Regarding the average speed of sound values (Table 3), calculated by

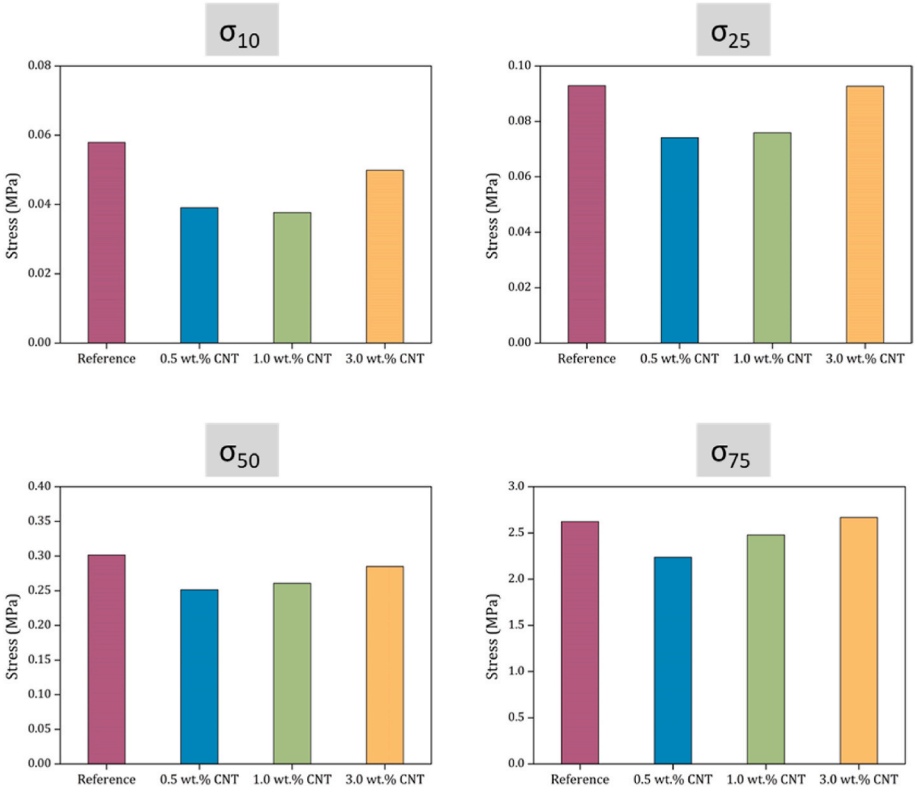

Fig. 7. Stress at different strains for all the aerogels.

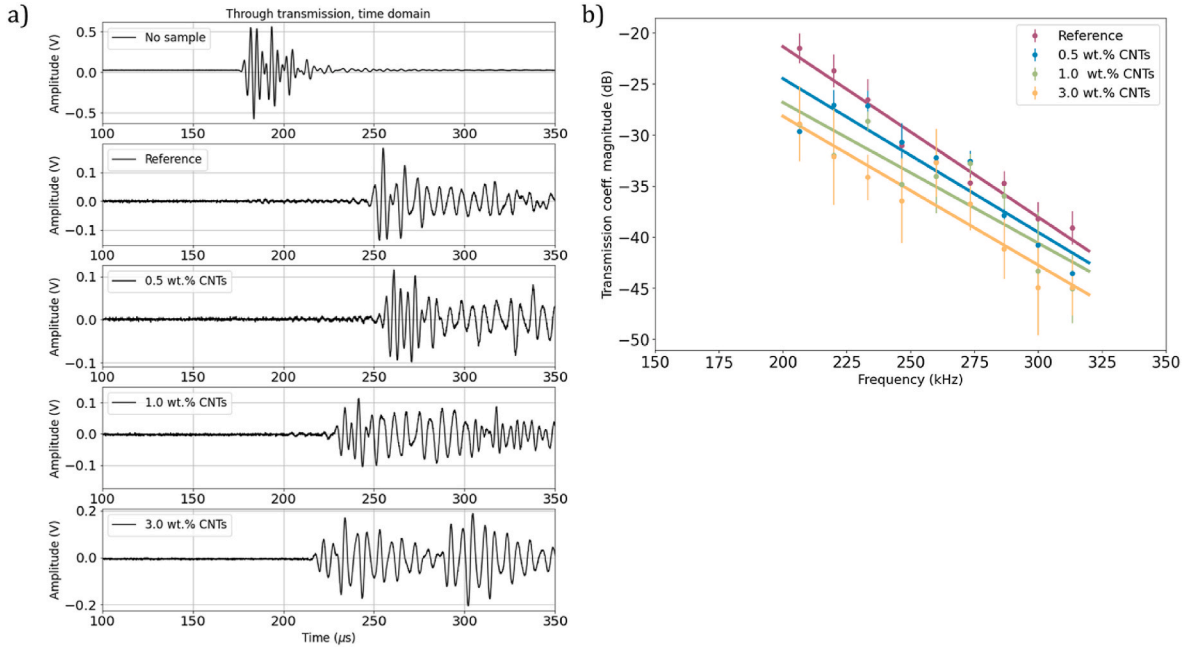

Fig. 8. a) Obtained signals in the time domain for the different aerogel formulations, b) Magnitude of the transmission coefficient vs frequency for the four aerogel samples.

employing the time of flight obtained through different methods (edge, cross-correlation, and phase spectrum slope) [35], they go from 110 m/s for the reference, to 101, 124 and 135 m/s for the aerogels with an increasing amount of carbon nanotubes (0.5 wt%, 1.0 wt% and 3.0 wt %). It is of interest the fact that ultrasonic loss increases with the content of CNTs while ultrasonic velocity increases too. Increase of velocity with the concentration of CNTs suggests that the presence of the CNTs contributes to create a stiffer structure at ultrasonic frequencies, while the higher loss is produced by an increase of the attenuation. The latter can be produced by a greater internal friction in the solid structure under the action of the ultrasonic wave. Thus, these fillers promote a more efficient sound attenuation while reaching higher sound speeds.

Table 3
Time of flight calculated by different methods and the average speed of sound for the different aerogels under study.

Sample	Tof (μs)			Average speed of sound (m/s)
	Edge method	Cross-correlation method	Phase spectrum slope method	
Reference	72	73.3	72.9	109.7 ± 0.6
0.5 wt% CNTs	78	79.2	79.2	101.0 ± 0.5
1.0 wt% CNTs	51	48.2	55.2	124.5 ± 5.0
3.0 wt% CNTs	39	40.5	46.6	134.7 ± 6.9

3.7. Thermal conductivity

The insulating performance of the produced aerogels has been studied by measuring their thermal conductivities by the stationary method. In order to evaluate the effect of the CNTs on the radiation contribution, thermal conductivity has been measured at different temperatures of 10, 20, 30 and 40 °C (experimental values can be found in Table S3 of Supporting Information).

The thermal conductivities obtained at 10 °C are plotted in Fig. 9. The results show that the value for the reference material is in the super-insulating region as showed in our previous work [36]. There is a noticeable decrease in the thermal conductivity values when different amounts of carbon nanotubes are added, that is more pronounced for higher CNT contents. The initial thermal conductivity of 15.07 mW/mK is reduced to 13.64 mW/mK when a low amount of CNTs is added (0.5 wt%) and further reduced for higher filler amounts reaching 12.46 mW/mK and 12.02 mW/mK for 1.0 and 3.0 wt% CNTs, respectively. The significant reductions of the thermal conductivity are also observed at high temperatures. A higher content of CNTs was included (5.0 wt%) showing that the thermal conductivity did not continue decreasing with a larger amount of this filler, probably because the percolation limit is reached, and pointing out that the 3.0 wt% content will be in the range of optimum content to reduce the thermal conductivity in this system.

Taking into account the heat transfer mechanisms in porous media, the different contributions to the total thermal conductivity (conduction through the solid phase λ_s, conduction through the gas phase λ_g, and radiation λ_r) can be calculated. The heat conduction mechanisms can be divided into solid and gas conduction (equations (11) and (12), respectively):

$$\lambda_s = \rho_r \cdot \lambda_s^{'} \cdot \frac{\upsilon}{\upsilon_s} \tag{11}$$

where ρ_r is the relative density, $\lambda_s^{'}$ is the thermal conductivity of the solid matrix (260 mW/mK [37]), and υ and υ_s are the speed of sound in the aerogel and solid matrix, respectively. The speed of sound of solid polyurethane υ_s has been taken as 1710 m/s [38]. The sound speed, υ, through the aerogel samples was that measured by using the described setup in section 2.4.10.

The gaseous contribution is calculated by taking into account the well-known Knudsen effect promoting a sharp decrease in the gaseous contribution when pores are in the nanometric scale [39,40]:

$$\lambda_g = (1-\rho_r)\cdot \lambda_g^{'} = (1-\rho_r)\cdot \frac{\lambda_{g0}^{'}(T)}{1+\frac{2\beta l_g}{\varphi_{pore}}} \tag{12}$$

Where λ'_{g0} is the thermal conductivity of the gas inside the pores (air), l_g is the mean free path of the gas molecules (c.a. 70 nm for air [40,41]), β is a correlation factor (1.64 for air [42]), and φ_{pore} is the average pore size.

The radiation contribution could be calculated using the following equation:

$$\lambda_r = \frac{16\cdot n^2 \cdot \sigma \cdot T^3}{3\cdot K_{e,R}} \tag{13}$$

where σ is the Stephan-Boltzmann constant (5.67×10^{-8} W/m^2 K^4), n is the refractive index, which is close to 1 for low density aerogels [38], $K_{e,R}$ the Rosseland extinction coefficient, and T is the mean temperature. However, since the carbon nanotubes added to the formulations should modify the extinction coefficient by absorption and scattering mechanisms, the radiation contribution has been quantitatively estimated by subtracting the solid and gas contributions (calculated by equations (11) and (12), respectively) from the experimental values.

The different contributions to the total thermal conductivity are plotted in Fig. 10. The main contribution to the thermal conductivity is the gaseous conduction along the aerogel pores which, as expected, slightly increased with the amount of carbon nanotubes since the pore size and the porosity also increased. This contribution rises from 9.35 mW/mK for the reference aerogel to 10.97 for the sample with the highest CNTs content.

Regarding the conduction through the solid phase, it depends on the phonon transfer through the polyurethane particulate skeleton. It is known that in aerogels the size effect takes place reducing the solid conduction in aerogels that is typically very small [43,44]. The observed differences between samples are mainly due to a different nanoporous structure: phonons are transmitted through the backbone structure, thus being the interparticle necks and particle connectivity key factors in this mechanism. In fact, the effect of the aerogel interruptions in the solid

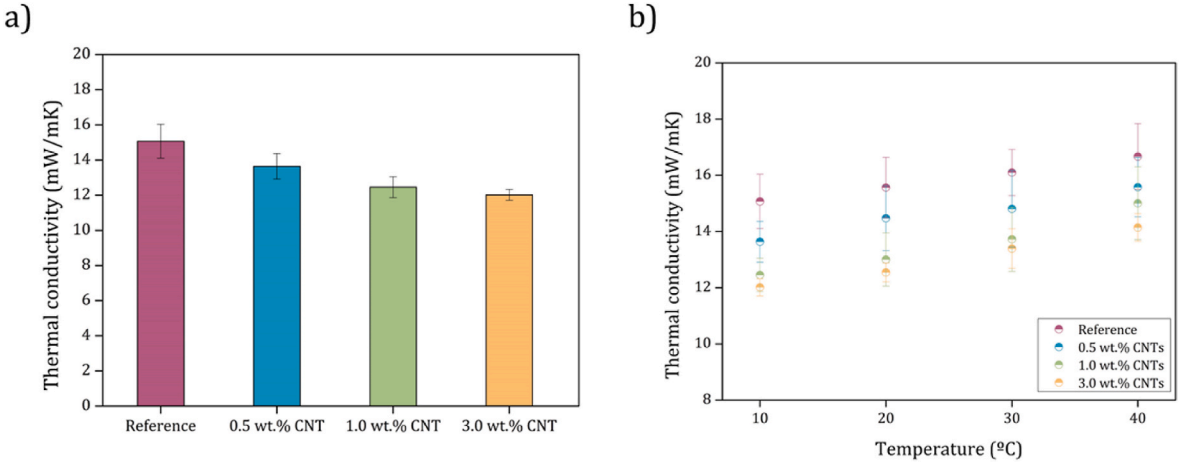

Fig. 9. Thermal conductivity values for the produced aerogels a) at 10 °C, and b) at different temperatures.

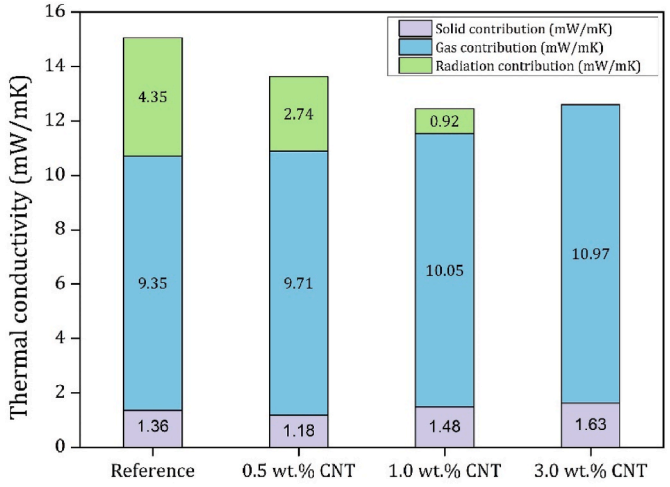

Fig. 10. Thermal conductivity contributions by subtracting the radiative term from the experimental value.

skeleton was demonstrated to have a strong dependence on the final thermal conductivity [45]. The ultrasound velocity in the aerogel is directly dependent on the phonon transfer through the particulated-strings of the aerogel. The obtained speed of sound through the samples (see Table 3) rises with an increasing amount of carbon nanotubes (0.5 wt%, 1.0 wt% and 3.0 wt%). This increase of the ultrasound velocity suggests that necks between particulated-strings of the aerogel are stiffer in the samples containing carbon nanotubes, which is consistent with the assumption that phonons would be less constrained in these samples and with the increase of the heat conduction through the solid phase. The contribution of this heat conduction mechanisms is below 2 mW/mK for all the materials considered (Fig. 10).

There is a sharp decrease in the radiative contribution by the addition of carbon nanotube opacifiers (Fig. 10) that act blocking the infrared radiation and obtaining reductions from 4.7 mW/mK to 2.74 mW/mK for the sample with 0.5 wt% CNTs, and 0.92 mW/mK for that containing 1.0 wt% of fillers. For the highest CNTs content (3.0 wt%) this term is remarkably reduced reaching an almost zero value. Therefore, the incorporation of CNTs is a very effective method to reduce the radiative heat transfer contribution for polyisocyanurate-polyurethane aerogels allowing to reach excellent insulating performances. This significant reduction compensates the increase of the conduction through the gas and solid phases, reducing the total conductivity of the aerogels.

4. Conclusions

Modified carbon nanotubes have been added as fillers in a polyisocyanurate-polyurethane aerogel formulation at different contents: 0.5, 1.0 and 3.0 wt%. The effect of these nanotubes on the structure and properties of the aerogels has been analyzed in detail:

The reaction kinetics were affected by the addition of CNTs. An increase in the gelation rate was detected when small amounts were added. However, when the nanotubes amount was further increased (3.0 wt%) similar gelation times than the reference were achieved.

The bulk density of these samples did not change significantly by the CNTs incorporation owing to the small concentrations added to the formulation. Nevertheless, the aerogel structure withstands better the drying step reducing the final shrinkage and therefore increasing the porosity of these aerogels. As a consequence, pores were slightly larger in the samples containing CNTs.

The scanning electron micrographs did not show any CNT agglomerate, thus confirming an effective dispersion of the fillers during the synthesis. Since the reference aerogel showed certain transparency to visible light, transmittance measurements were carried out to study the influence of carbon nanotubes on this property. Owing to the absorption and scattering produced by these fillers, the initial transmittance values were sharply reduced by the addition of CNT particles.

Regarding the mechanical properties of the nanocomposites, the enlarging of the pores forming the structure in combination with a different particle topology, led to a smaller stiffness and, therefore, reduced elastic moduli. Nevertheless, the elasticity and recovery of these samples, measured by the energy loss coefficient, was notably improved. Despite stiffness was worsen with the CNTs addition, none of the aerogels was broken at high deformations, allowing to be deformed until more than 80 % of strain with the subsequent densification.

Finally, the insulating performance was evaluated by the steady-state technique at different temperatures. A significant reduction of the thermal conductivity was achieved when the nanotubes were added decreasing from 15.07 mW/mK to 12.02 mW/mK for a CNTs content of 3.0 wt% at a temperature of 10 °C. The different heat transfer mechanisms were theoretically calculated obtaining the following conclusions:

- The gas conduction contribution was slightly increased (from 9.35 to 10.97 mW/mK) due to the larger pore size and higher porosity that aerogels showed when CNTs were added.
- The solid conduction contribution was increased as a consequence of a higher particle connectivity with the inclusion of CNTs on the aerogel structure and, therefore, phonon transfer was less restricted, as it was detected by the speed of sound measurements.
- The infrared radiation was significantly blocked by these nanotubes acting as opacifiers. An almost fully blockade of the heat transfer by radiation was obtained for a 3 wt% of CNTs confirming the effectiveness of these fillers to absorb and scatter the infrared radiation and the successful interactions with the aerogel matrix.

As main conclusion, adding a 3.0 wt% of CNTs in this aerogel system leads to a 20 % reduction in the thermal conductivity by decreasing the radiative contribution to almost zero. This excellent insulating material with 12 mW/mK of thermal conductivity, also shows lightweight (89.4 kg/m^3) and high porosity (92.4 %) while keeping a similar mechanical stiffness than the pure aerogel, having significantly high values of elastic modulus (0.46 MPa). The CNTs-polyisocyanurate-polyurethane aerogel composites herein synthesized can be proposed for a wide range of applications where low-density, high porosity, good mechanical strength and thermal insulation are key properties.

Credit author statement

Conceptualization, Beatriz Merillas, Tomás Gómez Alvarez-Arenas, Fernando Villafañe, and Miguel Rodríguez-Pérez; Data curation, Beatriz Merillas; Formal analysis, Beatriz Merillas; Funding acquisition, Fernando Villafañe and Miguel Rodríguez-Pérez; Investigation, Beatriz Merillas; Methodology, Beatriz Merillas, Tomás Gómez Alvarez-Arenas, and Miguel Rodríguez-Pérez; Project administration, Fernando Villafañe and Miguel Rodríguez-Pérez; Resources, Fernando Villafañe and Miguel Rodríguez-Pérez; Software, Beatriz Merillas; Supervision, Fernando Villafañe and Miguel Rodríguez-Pérez; Validation, Beatriz Merillas, Fernando Villafañe, Tomás Gómez Alvarez-Arenas and Miguel Rodríguez-Pérez; Visualization, Beatriz Merillas, Fernando Villafañe, Tomás Gómez Alvarez-Arenas and Miguel Rodríguez-Pérez; Writing – original draft, Beatriz Merillas; Writing – review & editing, Beatriz MerillasFernando Villafañe, Tomás Gómez Alvarez-Arenas and Miguel Rodríguez-Pérez.

Funding

Financial support from the FPU grant FPU17/03299 (Beatriz Merillas) from the Ministerio de Ciencia, Innovación y Universidades is grateful acknowledged. Financial assistance from Ministerio de Ciencia, Innovación y Universidades (MCIU) (Spain) (PID2021-127108OB-I00,

TED2021-130965B–I00 and PDC2022-133391-I00), Regional Government of Castilla y León and the EU-FEDER program (CLU-2019-04 and VA202P20) are gratefully acknowledged. This work was supported by the Regional Government of Castilla y León (Junta de Castilla y León), and by the Ministry of Science and Innovation MICIN and the European Union NextGenerationEU/PRTR. (C17. I1).

Declaration of competing interest

The authors declare that they have no known competing financial interests or personal relationships that could have appeared to influence the work reported in this paper.

Data availability

Data will be made available on request.

Acknowledgements

The authors would like to thank María Dolores Marqués Gutiérrez, from the Porous Solids Laboratory of the University of Malaga, for the nitrogen adsorption measurements, the Unidad de Microscopía of the Parque Científico of the University of Valladolid, for the HR-SEM and TEM images.

Appendix A. Supplementary data

Supplementary data to this article can be found online at https://doi.org/10.1016/j.mtchem.2023.101789.

References

[1] A. Soleimani Dorcheh, M.H. Abbasi, Silica aerogel; synthesis, properties and characterization, J. Mater. Process. Technol. 199 (1) (2008) 10–26.
[2] X. Li, Q. Wang, H. Li, H. Ji, X. Sun, J. He, Effect of sepiolite fiber on the structure and properties of the sepiolite/silica aerogel composite, J. Sol. Gel Sci. Technol. 67 (3) (2013) 646–653.
[3] X. Zhang, R. Zhang, C. Zhao, Ultra-small sepiolite fiber toughened alumina aerogel with enhanced thermal stability and machinability, J. Porous Mater. 27 (2020) 1535–1546.
[4] C. Simon-Herrero, L. Gomez, A. Romero, J.L. Valverde, L. Sanchez-Silva, Nanoclay-based PVA aerogels: synthesis and characterization, Ind. Eng. Chem. Res. 57 (2018) 6218–6225.
[5] T. Linhares, M.T. Pessoa De Amorim, L. Durães, Silica aerogel composites with embedded fibres: a review on their preparation, properties and applications, J. Mater. Chem. A 7 (40) (2019) 22768–22802.
[6] Z. Li, X. Cheng, S. He, X. Shi, L. Gong, H. Zhang, Aramid fibers reinforced silica aerogel composites with low thermal conductivity and improved mechanical performance, Compos. Part A Appl. Sci. Manuf. 84 (2016) 316–325.
[7] D. Loche, L. Malfatti, D. Carboni, V. Alzari, A. Mariani, M.F. Casula, Incorporation of graphene into silica-based aerogels and application for water remediation, RSC Adv. 6 (71) (2016) 66516–66523.
[8] S. Dervin, Y. Lang, T. Perova, S.H. Hinder, S.C. Pillai, Graphene oxide reinforced high surface area silica aerogels, J. Non-Cryst. Solids 465 (2017) 31–38.
[9] A. Lamy-Mendes, A.V. Girão, R.F. Silva, L. Durães, Polysilsesquioxane-based silica aerogel monoliths with embedded CNTs, Microporous Mesoporous Mater. 288 (2019), 109575.
[10] A. Lamy-Mendes, W.J. Malfait, A. Sadeghpour, A.V. Girão, R.F. Silva, L. Durães, Influence of 1D and 2D carbon nanostructures in silica-based aerogels, Carbon N. Y. 180 (2021) 146–162.
[11] M. Piñero, et al., Reinforced silica-carbon nanotube monolithic aerogels synthesised by rapid controlled gelation, J. Sol. Gel Sci. Technol. 86 (2) (2018) 391–399.
[12] M. Teymouri, M. Kokabi, G. Alamdarnejad, Conductive shape-memory polyurethane/multiwall carbon nanotube nanocomposite aerogels, J. Appl. Polym. Sci. 137 (2020), 48602.
[13] N. Kouklin, M. Tzolov, D. Straus, A. Yin, J.M. Xu, Infrared absorption properties of carbon nanotubes synthesized by chemical vapor deposition, Appl. Phys. Lett. 85 (19) (2004) 4463–4465.
[14] A.M. Gheitaghy, A. Ghaderi, S. Vollebregt, M. Ahmadi, R. Wolffenbuttel, G. Q. Zhang, Infrared absorbance of vertically-aligned multi-walled CNT forest as a function of synthesis temperature and time, Mater. Res. Bull. 126 (2020), 110821.
[15] D. Baillis, R. Coquard, Radiative and conductive thermal properties of foams, in: Cellular and Porous Materials: Thermal Properties Simulation and Prediction, 2008, pp. 343–384.
[16] M. Santiago-Calvo, et al., Evaluation of the thermal conductivity and mechanical properties of water blown polyurethane rigid foams reinforced with carbon nanofibers, Eur. Polym. J. 108 (2018) 98–106.
[17] C. Tan, B.M. Fung, J.K. Newman, C. Vu, Organic aerogels with very high impact strength, Adv. Mater. 13 (9) (2001) 644–646.
[18] M.T. Kim, K.Y. Rhee, S.J. Park, D. Hui, Effects of silane-modified carbon nanotubes on flexural and fracture behaviors of carbon nanotube-modified epoxy/basalt composites, Compos. Part B Eng. 43 (2012) 2298–2302.
[19] B. Merillas, J. Martín-de León, F. Villafañe, M.A. Rodríguez-Pérez, Transparent polyisocyanurate-polyurethane-based aerogels: key aspects on the synthesis and their porous structures, ACS Appl. Polym. Mater. 3 (9) (2021) 4607–4615.
[20] ASTM D1622-08: Standard Test Method for Apparent Density of Rigid Cellular Plastics. West Conshohocken, PA, USA: ASTM International, 2008.
[21] L. Juhász, et al., False morphology of aerogels caused by gold coating for sem imaging, Polymers 13 (4) (2021) 1–12.
[22] J. Pinto, E. Solórzano, M.A. Rodriguez-Perez, J.A. De Saja, Characterization of the cellular structure based on user-interactive image analysis procedures, J. Cell. Plast. 49 (6) (2013) 555–575.
[23] E.P. Barrett, L.G. Joyner, P.P. Halenda, The determination of pore volume and area distributions in porous substances. I. Computations from nitrogen isotherms, J. Am. Chem. Soc. 73 (1) (1951) 373–380.
[24] ASTM C518, Standard Test Method for Steady-State Thermal Transmission Properties by Means of the Heat Flow Meter Apparatus, 2017. West Conshohocken, PA, USA.
[25] ISO 8301:1991- Thermal Insulation — Determination of Steady-State Thermal Resistance and Related Properties — Heat Flow Meter Apparatus, 1991. Geneva, Switzerland.
[26] I. Sánchez-Calderón, B. Merillas, V. Bernardo, M.Á. Rodríguez-Pérez, Methodology for measuring the thermal conductivity of insulating samples with small dimensions by heat flow meter technique, J. Therm. Anal. Calorim. 147 (2022) 12523–12533.
[27] ASTM D1621–00 Standard Test Method for Compressive Properties of Rigid Cellular Plastics. West Conshohocken, PA, USA, 1991.
[28] ISO 291:2005 Plastics — Standard Atmospheres for Conditioning and Testing," Geneva, Switzerland, 2005.
[29] J. Bhinder, P.K. Agnihotri, Effect of carbon nanotube doping on the energy dissipation and rate dependent deformation behavior of polyurethane foams, J. Cell. Plast. 57 (2020) 287–311.
[30] C.J. Brinker, G.W. Scherer, Sol-Gel Science: the Physics and Chemistry of Sol-Gel Processing, Academic Press, Oxford, UK, 1990.
[31] R. Al-Oweini, H. El-Rassy, Synthesis and characterization by FTIR spectroscopy of silica aerogels prepared using several Si(OR)4 and R″Si(OR')3 precursors, J. Mol. Struct. 919 (2009) 140–145.
[32] B. Merillas, J. Martín-de León, F. Villafañe, M.Á. Rodríguez-Pérez, Optical properties of polyisocyanurate – polyurethane aerogels : study of the scattering mechanisms, Nanomaterials 12 (2022) 1522.
[33] S. Aney, A. Rege, The effect of pore sizes on the elastic behaviour of open-porous cellular materials, Math. Mech. Solids 28 (7) (2023) 1624–1634.
[34] L. Ratke, A. Rege, S. Aney, The effect of particle necks on the mechanical properties of aerogels, Materials 16 (1) (2023) 1–12.
[35] D.R. Hull, H.E. Kautz, A. Vary, Ultrasonic Velocity Measurement Using Phase-Slope and Cross- Correlation Methods, 1984.
[36] B. Merillas, F. Villafañe, M.Á. Rodríguez-Pérez, Super-insulating transparent polyisocyanurate-polyurethane aerogels: analysis of thermal conductivity and mechanical properties, Nanomater 12 (2022). Page 2409, vol. 12, no. 14, p. 2409, Jul. 2022.
[37] S. Estravís, J. Tirado-Mediavilla, M. Santiago-Calvo, J.L. Ruiz-Herrero, F. Villafañe, M.Á. Rodríguez-Pérez, Rigid polyurethane foams with infused nanoclays: relationship between cellular structure and thermal conductivity, Eur. Polym. J. 80 (2016) 1–15.
[38] L.W. Hrubesh, R.W. Pekala, Thermal properties of organic and inorganic aerogels, J. Mater. Res. 9 (3) (1994) 731–738.
[39] M.A. Aegerter, N. Leventis, M.M. Koebel, Aerogels Handbook, Springer, Berlin, Germany, 2011.
[40] B. Notario, J. Pinto, E. Solorzano, J.A. De Saja, M. Dumon, M.A. Rodríguez-Pérez, Experimental validation of the Knudsen effect in nanocellular polymeric foams, Polymer (Guildf). 56 (2015) 57–67.
[41] C. Forest, P. Chaumont, P. Cassagnau, B. Swoboda, P. Sonntag, Polymer nano-foams for insulating applications prepared from CO2 foaming, Prog. Polym. Sci. 41 (C) (2015) 122–145.
[42] S. Song, M.M. Yovanovich, F.O. Goodman, Thermal gap conductance of conforming surfaces in contact, J. Heat Tran. 115 (3) (1993) 533–540.
[43] J. F, R.W.P.X. Lu, M.C. Arduini-Schuster, J. Kuhn, O. Nilsson, Thermal conductivity of monolithic organic aerogels, Science 255 (5047) (2016) 971–972.
[44] Z. Zhang, Y. Ouyang, Y. Cheng, J. Chen, N. Li, G. Zhang, Size-dependent phononic thermal transport in low-dimensional nanomaterials, Phys. Rep. 860 (2020) 1–26.
[45] B. Merillas, J.P. Vareda, J. Martín-de León, M.Á. Rodríguez-Pérez, L. Durães, Thermal conductivity of nanoporous materials: where is the limit? Polymers 14 (13) (2022) 2556.